SURFACE MECHANICS OF POLYACRYLAMIDE HYDROGELS FOLLOWING WEAR

BY

MICHAEL ATTEN

THESIS

Submitted in partial fulfillment of the requirements
for the degree of Master of Science in Mechanical Engineering
in the Graduate College of the
University of Illinois at Urbana-Champaign, 2018

Urbana, Illinois

Adviser:

Assistant Professor Alison C. Dunn

ABSTRACT

In this work, the changes in elasticity of synthetic hydrogel surfaces following deliberate abrasive surface wear are measured. These polyacrylamide hydrogels – cross-linked polymers consisting of 92% water by mass – undergo surface wear, and their surface elastic properties before and after wear are measured. Quasi-static nanoindentations are performed on the surface using a colloidal probe in an atomic force microscope (AFM), and the elastic modulus is computed from the region of the curves fitting a Hertzian contact regime. The results show that the surfaces are stiffer directly after wear. These changes are recoverable, and after several days of resting underwater, the hydrogel's surface stiffness characteristics return to similar values as before any wear is applied. From this, it can be deduced that wear removes a soft, swollen surface layer and reveals a stiffer bulk. Surfaces can undergo further wear and re-swell successfully with every repetition of the experiment. This research in surface mechanics of hydrogels after applied surface wear is applicable to load-bearing hydrogel surfaces in the human body.

ACKNOWLEDGMENTS

I would like to express my sincere gratitude toward the following people, without whose help and support this thesis would not be possible. First and foremost, to my adviser, Professor Alison C. Dunn, who gave constant guidance and discerning feedback. To Yijue Diao and Professor Rosa M. Espinosa-Marzal, for use of their lab facilities and for teaching me to make my own colloidal probes. To Scott Maclaren, who initially taught me to use an AFM, and to Kathy Walsh who provided endless troubleshooting advice. A portion of this work was carried out in part in the Frederick Seitz Materials Research Laboratory Central Research Facilities, University of Illinois.

TABLE OF CONTENTS

CHAPTER 1: INTRODUCTION

Hydrogels are three-dimensional, cross-linked networks of water-soluble polymers [1]. They are often more than 90% water and are relatively soft as a result. This makes their surface properties difficult to measure. The water stored inside the network flows in response to loading conditions [2]. This can change the concentration of water at the surface, and therefore the mechanical properties, so low contact pressures are necessary to prevent redistribution of the water content at the surface [3].

Hydrogels see use in a variety of medical applications, including electrophoresis cells, cell culture substrates, contact lenses, burn dressings, dentures, and drug delivery systems [4]. Their high water content aids their biocompatibility, and their soft consistency shows a strong resemblance to soft tissue [5]. One of the main limitations with using hydrogels in the body is their poor mechanical properties. Attempts at creating tissue substitutes with hydrogels have yielded results with significantly poorer mechanical strength than the real tissues [6]. An area that does show some promise is the use of synthetic compliant materials for articulating surfaces of replacement joints. Hydrogels at this interface would reduce contact stresses and encourage a fluid film lubrication mechanism [7].

One primary obstacle to full implementation of hydrogels as load-bearing tissue replacements is that their wear behavior in repeated sliding is not known. There have been several studies on the frictional response of gels, and the coefficient of friction is well characterized [8], [9], [10], [11], however, a 2000 study found no correlation between friction and wear [12], indicating the importance of studying the wear behavior of hydrogels independently. Low friction does not necessarily imply low wear.

Quantifying the wear of these swollen polymers is difficult to define because of their low modulus and the interaction of the chains in the network. One way to interpret the wear is through a contact mechanics-based approach like Archard's equation [13], which is based on a theory of asperity contact. These contacting asperities between two surfaces in relative motion can lead to abrasive wear, which refers to the removal of material from the surface due to the presence of hard particles between two contacting surfaces [14]. A 1969 study found that as the surface applying wear becomes smoother, the wear process changed from cutting on an asperity scale to surface fatigue. Fatigue was also more pronounced in more elastic polymers [15].

Polymer wear can also be interpreted from a standpoint of bond breakage, wherein the bonds between the network chains are sundered [16]. The breakage of these covalent bonds generally results in the formation of radicals [17]. Once the radicals are formed, they tend to react with their surroundings to seek a lower energy state by forming new covalent bonds. These subsequent reactions prevent most tough hydrogels from self-healing because the covalent sacrificial bonds cannot re-form [18]. Some researchers have been able to make self-healing tough hydrogels by replacing the brittle covalent networks with easily re-formable non-covalent bonds [19].

The variety of approaches and the lack of a unifying theory make the wear behavior of hydrogels difficult to interpret. This lack of understanding is a primary hurdle to implementation of hydrogels as tissue replacements [20]. This thesis examines polyacrylamide hydrogels and their mechanical response to applied abrasive wear. It quantifies the stiffness changes at the surface and ultimately proposes a mechanism to explain the observations. This research in applied surface wear has uncovered unexpected surface mechanics that may be applicable to synthetic hydrogels employed in load-bearing applications within the human body.

CHAPTER 2: MATERIALS AND METHODS

This chapter describes the samples used in the wear experiments, including sample preparation and recipe selection and optimization. It details the specifications of how the experiments were performed, including information about the colloidal probes used to characterize the samples and the procedure for abrasively wearing the samples. Finally, there is a discussion of how the wear behavior of hydrogels over time is investigated through longitudinal experiments.

2.1 Sample preparation

The hydrogel sample was polymerized 24 hours before experimentation. The process of creating a sample included gentle mixing a pre-polymerization liquid mixture to prevent the introduction of air pockets, pouring the liquid mixture into a shallow petri dish 40 mm in diameter that served as the sample holder in subsequent experiments, and molding with a flat plastic cover to ensure the surface of the polymerized sample was as smooth as possible. Once the polymerization process was finished, the cover was carefully removed, the gel was rinsed to remove any unpolymerized liquid still on the surface, and the hydrogel was stored under water in the fridge overnight [21].

To select the recipe for the hydrogels used in these experiments, a few different criteria were considered. The resultant gel had similar characteristics to naturally occurring biomaterials, which allowed for consideration of the hydrogel's usefulness as a biomaterial substitute [20]. The gel recipe was prevalent across a wide breadth of researchers, which allowed for comparison of its properties to those others have found [22]. Finally, the gel polymerized quickly and was stable for an extended period, which allowed for rapid experimentation and evaluation of the same sample in longitudinal experiments. To fit these criteria, a recipe of 7.5 wt.% acrylamide monomer (Aam), 0.39 wt.% bis-acrylamide crosslinker (Bis), and 92 wt.% water was used. Polymerization was

achieved through the addition of the initiator and radical donor, 0.05 wt.% ammonium persulfate (APS) and 0.15 wt.% tetramethylethylenediamine (TEMED).

2.2 Crosslinker Experiments

The relative amount of monomer and crosslinker was an important factor to consider. The amount of bis-acrylamide was optimized through a series of experiments that measured the degree of swelling different hydrogel recipes experience over time. The amount of water either absorbed or desorbed was found by careful measurement of both the sample weight and physical dimensions. The highest monomer to crosslinker ratio of 25:1 resulted in pronounced swelling of the sample over time (swelling ratio $Q > 1$) and led to the gel bulging out of its holder during experiments. This recipe made a gel that increased in mass 3.2% over a week. The smallest ratio of 18:1 produced an artificially-stiff sample [22]. The gels made with this ratio shrank over time, decreasing in mass by 2.2% over the course of a week ($Q < 1$). The sample that exhibited a swelling ratio of $Q = 1$ was deemed the most stable [23], and that recipe was used for all experiments.

2.3 Probe Specifications

The colloidal probes used in these experiments had a 5 μm diameter borosilicate sphere attached at the tip. In early experiments, pre-fabricated silicon nitride probes (Novascan, IA, USA) with a measured stiffness $k = 0.1\ \mathrm{N/m}$ were used. This relatively low stiffness was chosen to achieve measurable forces during small-depth indentations of the sample [24]. In later experiments, colloidal probes were constructed by attaching a silica microsphere (Bangs Labs, IN, USA) on a cantilever probe (NanoAndMore, CA, USA) using a quick-dry epoxy (Bangs Labs, IN, USA). A diluted solution of colloids was dehydrated [25], and an individual particle was placed on the probe tip using a micromanipulator [10].

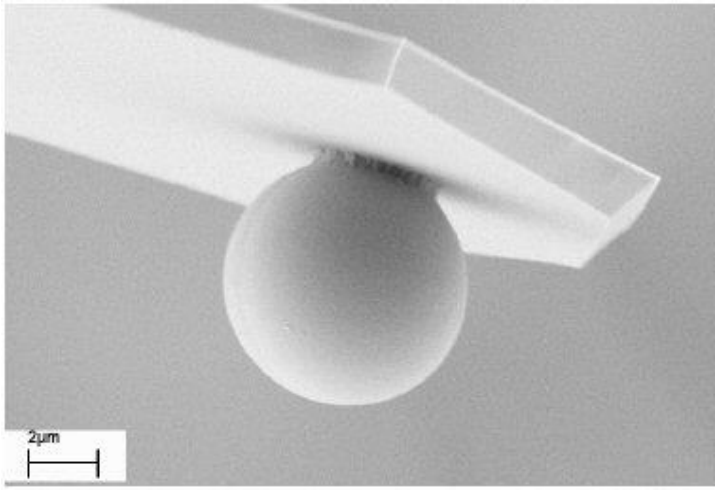

Figure 2.1. Colloidal probe with a 5 µm diameter sphere attached to the tip used in indentation experiments [26].

2.4 Experimental Procedure

The soft transparent surface and the need to keep the hydrogel under water during the indentation tests all increased the difficulty of measuring the surface properties with the atomic force microscope (MFP3D, Asylum Research, Santa Barbara, USA). To mitigate these challenges, some techniques were developed. The first was to create a gel that was smaller than the height of the sample holder. The polymerized gel height was 1 mm, so there was space in the dish for water on top of the sample during testing (Figure 2.2).

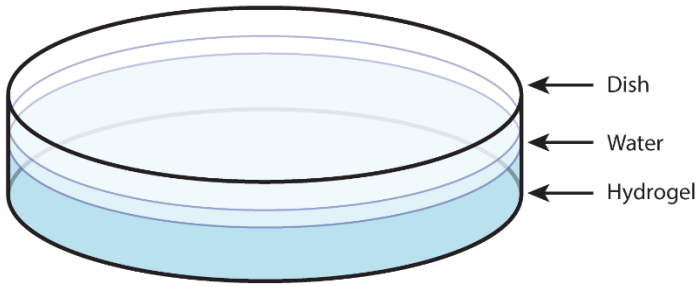

Figure 2.2. Sample holder setup. The hydrogel fills half of the petri dish (1 mm in height). A small amount of water is added to the top of the hydrogel to keep it hydrated during experiments.

A balance was struck between making the gel height small enough, so an adequate amount of water could be added to the dish but large enough so that deformations on the surface could be treated as isolated to the surface region. Indentation depths were minor compared to the overall sample depth [27], comprising less than 1% of the total height of the hydrogel. Any amount of time the hydrogel remained out of water, noticeable dehydration occurred, so attempts to quickly measure surface properties in air were impossible. Safety precautions were taken to protect the sensitive electronics in the AFM from spilled water, and the probe was pre-wetted to ease the insertion into the water.

The probe was calibrated in a standard fashion by measuring the inverse optical lever sensitivity (InvOLS) by performing a force curve on a hard surface in air and again on a hard surface in fluid. The stiffness (k = 0.1 N/m) was confirmed using the thermal method [28]. The outside of the petri dish sample holder was glued to a glass microscope slide and clamped down to the AFM stage to securely hold the hydrogel and prevent any motion during the lateral movements of the probe.

To locate the surface, the probe was slowly lowered until minimum contact was made. The probe was then raised slightly above the surface, and the experiment could begin. If the probe remained embedded in the surface before the experiment, there were two issues that could arise. First, sustained application of a normal force into the hydrogel surface would result in gradual deformation of the body [29]. As the gel relaxed, the measured force would decrease, or the machine would not reach the pre-load threshold once it raised and lowered the probe. A secondary issue was the possibility of the probe remaining embedded in the sample over the course of the experiment. If the probe was not raised above the sample at the beginning of the test, there would not be adequate vertical clearance for it to disengage from the surface, move to the next location,

and repeat the indent process. Instead, the probe would be dragged through the top layer of the gel, skewing the results and potentially damaging the probe. To mitigate these dangers, the probe was raised an appropriate distance above the surface, and the vertical motion of the probe during the indents was set to its maximum value of 12 µm [28]. The hydrogels were indented with a force up to 50 nN and depths less than 3 µm.

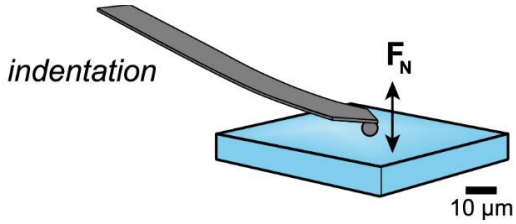

Figure 2.3. Method used to characterize hydrogel samples. Indentation was performed at the nanoscale using colloidal probe atomic force microscopy.

To characterize a large portion of the hydrogel surface, maps of 100 force indents were performed, shown in Figure 2.4. These maps consisted of a 10 x 10 array of force curves in a 90 µm x 90 µm square [30]. Two force maps were done on every sample for a total of 200 force curves across a wide area of the surface. The scan rate was set to 1 Hz and the indentation rate of the probe was 23 µm/s. Force vs. indentation depth data was exported to an Excel file for analysis in MATLAB.

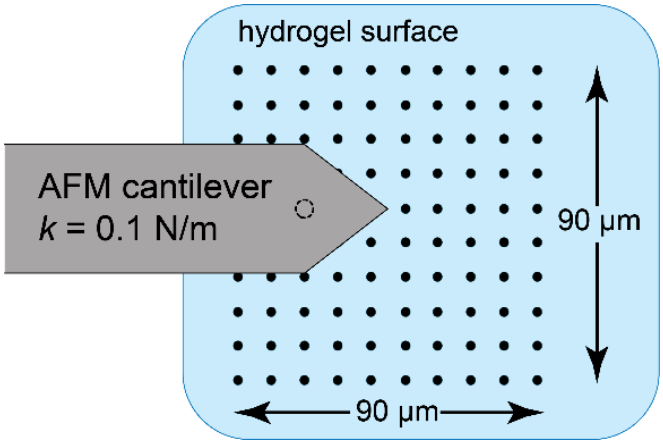

Figure 2.4. Schematic map showing the input locations for each of 100 quasistatic nanoindentation measurements on the hydrogel surface over an area of 90 µm x 90 µm.

2.5 Wear Experiments

To quantify how wear affected the hydrogel surface, a series of wear experiments were performed. These experiments consisted of the following procedure: (i) a fresh, unworn hydrogel made 24 hours prior was placed in the AFM; (ii) two force maps of 100 force curves each were performed across the unworn surface; (iii) the sample was removed from the AFM and worn abrasively by reciprocating 1000 grit sandpaper under a light hand load across the surface; (iv) the sample was thoroughly rinsed with DI water to remove debris; (v) the sample was again placed in the AFM and another set of 200 force curves were made across the surface. This procedure allowed direct comparison of a sample pre- and post-wear. It was possible to observe and quantify immediate effects of abrasive wear.

2.6 Longitudinal Experiments

In order to understand how the hydrogel properties changed after repeated applications of wear, a set of longitudinal experiments was initiated. The purpose of these experiments was to discern if the hydrogel properties changed as the sample aged and if the hydrogel had an opportunity to recover after being worn. The procedure for these experiments was as follows: (i) a set of two hundred force curves was mapped across the surface of a fresh, unworn hydrogel made 24 hours prior; (ii) the sample was removed from the AFM and worn abrasively using 1000 grit sandpaper, and debris was rinsed away; (iii) the sample was re-tested with another set of 200 force curves across the surface; (iv) the sample was stored underwater at 4°C for 72 hours; (v) the aged sample again underwent a set of indentation tests across the surface; (vi) the sample was worn again with 1000 grit sandpaper, was rinsed, and then underwent another set of force curves. This procedure was conducted multiple times, demonstrated in Figure 2.5. The longitudinal experiments took place over three stages. This means that the gel was worn three separate times, and its elastic properties were characterized on three different days over the course of a week, detailed by the procedure above.

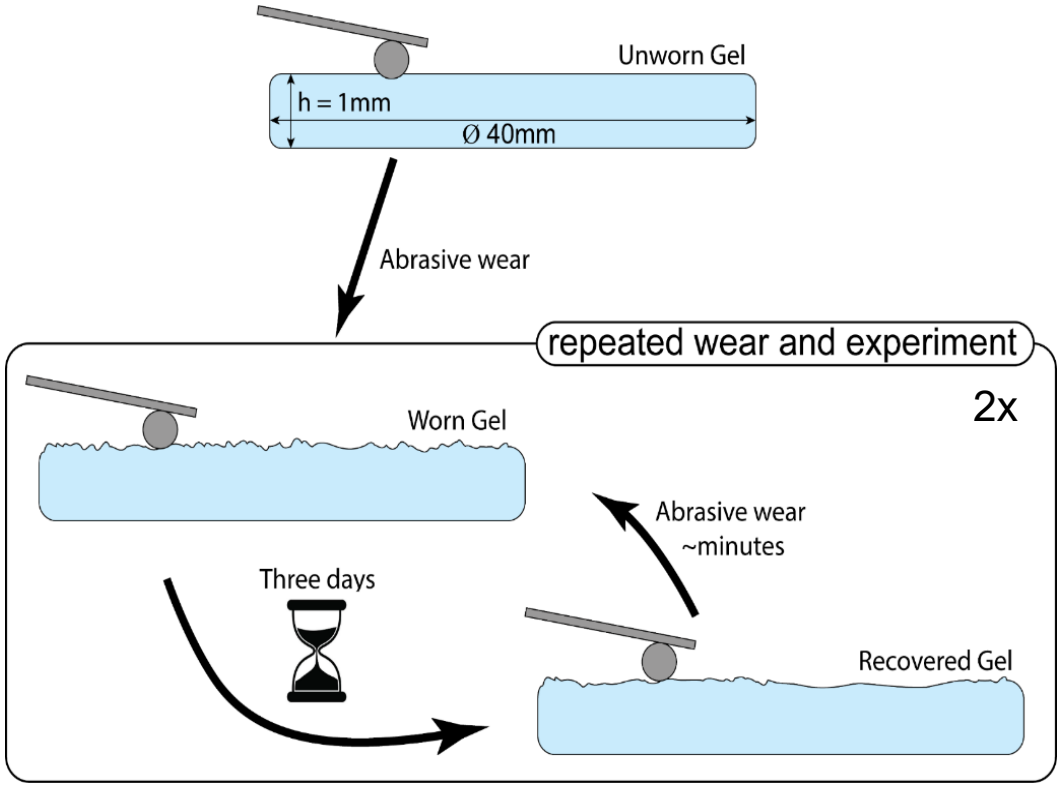

Figure 2.5. One experiment follows this longitudinal progression. The experiment was repeated up to three times on the same sample such that the same area was worn multiple times and characterized before and after each application of wear. The pre-wear and post-wear characterization consisted of quasistatic nanoindentation using the AFM. All characterization was done within the worn area and repeated multiple times to assess repeatability. Finally, the samples were allowed to recover for 72 hours submerged in water before the next experiment.

CHAPTER 3: DATA ANALYSIS

This chapter details the procedure used to analyze the data collected from the AFM. It presents a discussion of the curve fitting process, including plots and the fitting model.

3.1 Analysis Procedure

During the experiment, the force and displacement data was gathered at an acquisition rate of 2 kHz [28], giving approximately 1000 data points per extension curve. The results from the 100 force curves in the force map can be seen in Figure 3.1, which overlays the force curves taken on a single sample.

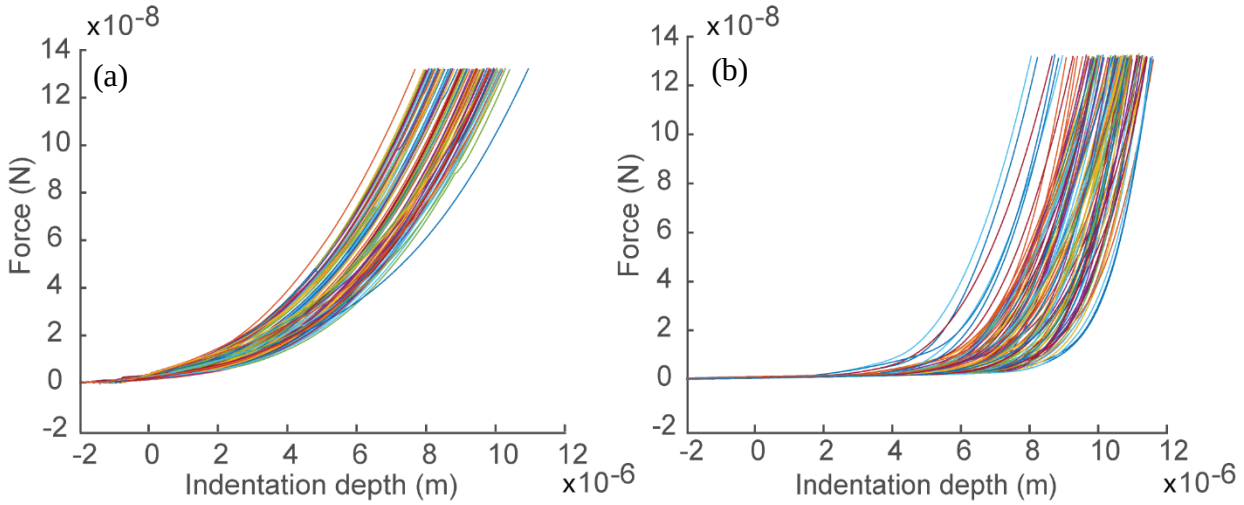

Figure 3.1. One hundred force curves from a force map on the hydrogel surface. (a) Curves from an unworn sample are shown on the left. (b) Curves from a worn sample are displayed on the right.

All force versus displacement curves were analyzed using MATLAB. A custom MATLAB code removed the data from the retraction portion of the force curve and displayed the extension portion. It then took a manual user input that identified the contact point between the sample and the probe and trimmed any data points corresponding to depth values less than the chosen contact point. Using a least-squares regression fit, the code compared the force curve data to a power law function and identified a region of interest that matched a Hertz model [31]

$$F = \frac{4}{3} R^{0.5} E^{*} \delta^{1.5}. \tag{3.1}$$

This theory models the contact of an elastic sphere of radius *R* indenting an elastic half-space to a depth δ. The applied force *F* is related to the indentation depth by a power of 1.5, and E^{*}, the effective modulus, is related to the Poisson ratios and elastic moduli associated with the particle tip and the hydrogel sample, shown in the equation [32]

$$\frac{1}{E^{*}} = \frac{1-\nu_1^2}{E_1} + \frac{1-\nu_2^2}{E_2}. \tag{3.2}$$

The borosilicate probe had values of $\nu = 0.17$, $E = 70$ GPa [33], and the hydrogel has a Poisson ratio of $\nu = 0.45$ [21]. Since the Young's modulus for the spherical tip was so much higher than the elastic modulus of the sample, the contribution from E_2 could be ignored, and

$$E^{*} = \frac{E_1}{1-\nu_1^2} = 1.25\, E_1 \tag{3.3}$$

After the code identified the portion of the force curve that followed a 1.5 power law relation, it fit this region to equation 3.1 with the effective modulus as the only free parameter, seen in Figure 3.2. This procedure is discussed in depth in the following section. Finally, the elastic modulus of the sample was computed with equation 3.2, and the process was repeated for all one hundred force curves.

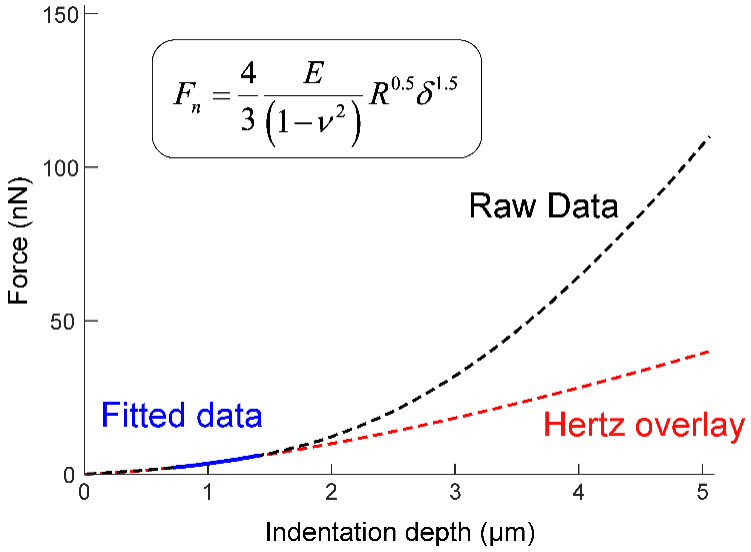

Figure 3.2. Quasistatic indentation at the nanoscale was fit over a shallow-depth region using the Hertz model to characterize the elastic response.

The fitting model chosen was a one-term power series given by $y = ax^b$ and was implemented in MATLAB. The coefficients *a* and *b* were found within a 95% confidence bound [34]. To evaluate the goodness of fit, MATLAB also calculated the sum of squares due to error (SSE), an R-square value, and a root mean square error (RMSE). For the representative sample shown in Figure 3.2, the blue fitted region had a coefficient of $b = 1.513$ with a 95% confidence interval of 1.503 to 1.523, R-square of 0.9995, SSE of 2.697, and RMSE of 0.1538.

3.2 Curve-Fitting Code

The MATLAB code used to analyze the force curve data from the AFM went through several iterations as various approaches were tried and discarded. The goal of the code was to trim the raw data by recognizing the contact point between the probe and the sample, identify and isolate the region of the curve that fit the Hertz model of an elastic half space indented by a spherical indenter, apply the fit, and extract the elastic modulus for each of 100 different force curves from a single experiment [29]. The challenge of creating a code that accomplished these

tasks efficiently and consistently was an ongoing one that required frequent iteration and improvement.

Initially, simple fitting methods were used, but the fits were poor, and uncertainties were too high to identify significant differences between pre- and post-wear measurements. This attempt at finding the elastic modulus used a simple solver to minimize the sum of the error. The values of the force vector were compared to force values from the Hertz model with an assumed elastic modulus as the free parameter. This modulus value was changed until the difference between the two force values was minimized. This method required constant guess-and-check and was quickly rejected.

To reduce the need for constant user input throughout the curve fitting process, an automatic fitting function was implemented to fit a curve or surface in x- and y-data vectors to a specified model [35]. The first iteration of the code defined two shifting parameters in both the x- and y-directions. These two degrees of freedom were used because of the nature of the force vs. indentation data. Since the surface of the sample changed after wear, each indent was performed with the maximum vertical motion of the probe (~12 μm). This precaution was taken to guarantee full interaction with any weaker asperities dangling from the surface as well as the bulk of the sample below, but it left the indentation curves with a large zero-force initial region as the probe traveled toward the surface. The two shifting parameters should have ideally helped the fitting function identify the point of contact between the probe and the sample, but this process was resource-intensive as MATLAB tried to balance three unknown parameters (elastic modulus, depth-shifting parameter, and force-shifting parameter). It was also ineffective at choosing the right starting point because a small local region of the curve matching the n~1.5 exponent in the

Hertz model could be found for a very large range of contact points. This false positive gave unrealistic modulus values and perhaps even started at forces that surpassed the pre-load threshold.

The next iteration of the fitting code used logarithmic functions to identify the region of interest within the Hertzian regime. It was important to find the portion of the curve where force was proportional to depth to the three-halves power $F \sim d^{1.5}$. By taking the logarithm of both sides and using the relation

$$\log(F) \sim 1.5 \log(d), \tag{3.4}$$

the area of the curve that fit the Hertz model would be one that had a linear slope of $m = 1.5$ between depth vs. force. To find this region, a simple linear fit $y = mx + b$ was applied to the log-log curve, and the region that fit a slope of 1.5 was found. This same linear fit was applied to ever-increasing intervals away from the center of this region such that the slope stayed within a tolerance of ± 0.1 $(1.4 < m < 1.6)$.

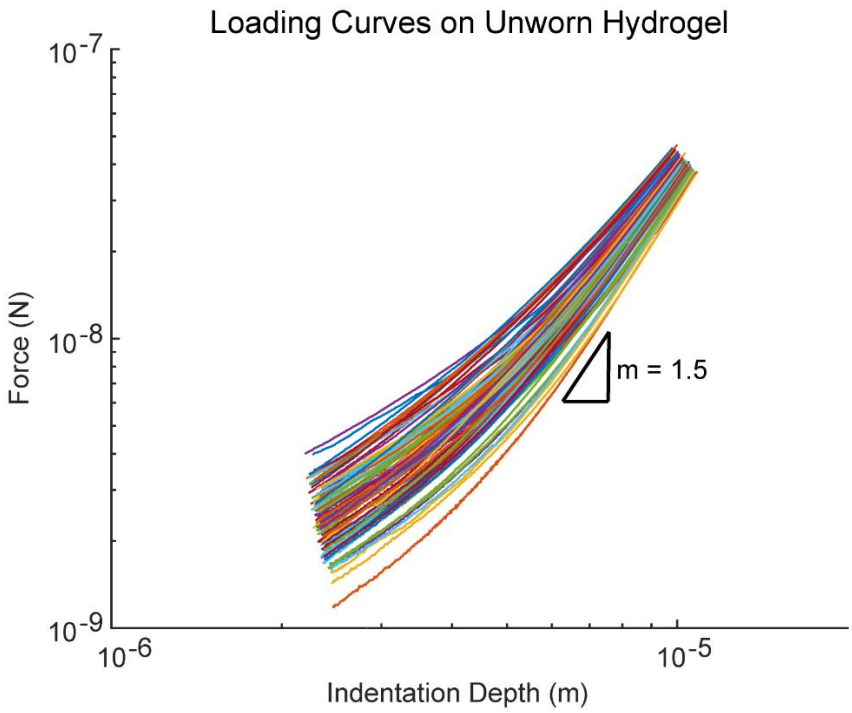

Figure 3.3. Iteration of curve fitting procedure in which the logarithms of both force and indentation depth are computed, and the region that has a slope of $m = 1.5$ is isolated for further analysis.

This region was then extracted from the larger data set and fit to the Hertz model, and the elastic modulus was extracted. This method was also time-consuming as the linear fitting function needed to continuously evaluate ever-larger data sets to determine the Hertz region. An attempt to speed this process involved using a box car to increment along the log-log curve. The box car method maintained a region of fit that was consistent in size and could successfully identify the end points of the region defined by a power of 1.5. The box car method significantly reduced the time necessary to evaluate an entire indentation curve.

Some issues arose with taking the logarithm of the force and depth vectors, particularly in the zero-force region at the beginning of the curve. While the force vector was initially trimmed of values corresponding to the zero-force measurement before contact, the noise floor of the

instrument meant that there was still some oscillation above and below zero. These negative values in the force vector led to errors when taking the log of both sides of the Hertz equation. The linear fit comparing a slope between force and depth was easy to implement, but the process of applying a logarithm ultimately made this method troublesome.

The next approach was to directly fit a power-law relationship to the curve. The depth vs. force columns were fit to a simple power law $y = ax^b$, and the region that the exponent b was within a ± 0.1 tolerance of 1.5 was identified and isolated. This region was fit to a Hertz model, and the elastic modulus was computed. This iteration of the curve fitting code was consistently successful, and the lessons of reducing the number of shifting parameters and using a box car to fit portions at a time were applied to speed up the processing time.

The final iteration removed the shifting parameter along the x-axis. MATLAB sometimes struggled with identifying the point of contact between the probe and the hydrogel. The noise in the force vector when measuring zero force occasionally caused selection of the wrong contact point as a false positive because of a small increase in the force measurement. The possibility of these mistakes required lengthy manual error-checking of each curve to ensure the integrity of the modulus values. In a compromise between more manual input in the beginning to save time error checking at the end, the MATLAB function "ginput" was implemented, seen in Figure 3.4. This function took a graphical input from a user's cursor. For each indentation curve, the contact point was manually identified, and all data points corresponding to depth-values smaller than this point were removed. Since MATLAB was given the correct contact point, the x-axis shifting parameter was no longer necessary. Three variables were reduced to a single variable of interest: the modulus of elasticity. While this final iteration required more manual interaction with the code, it saved time over all and reduced errors compared to the more automatic fitting functions.

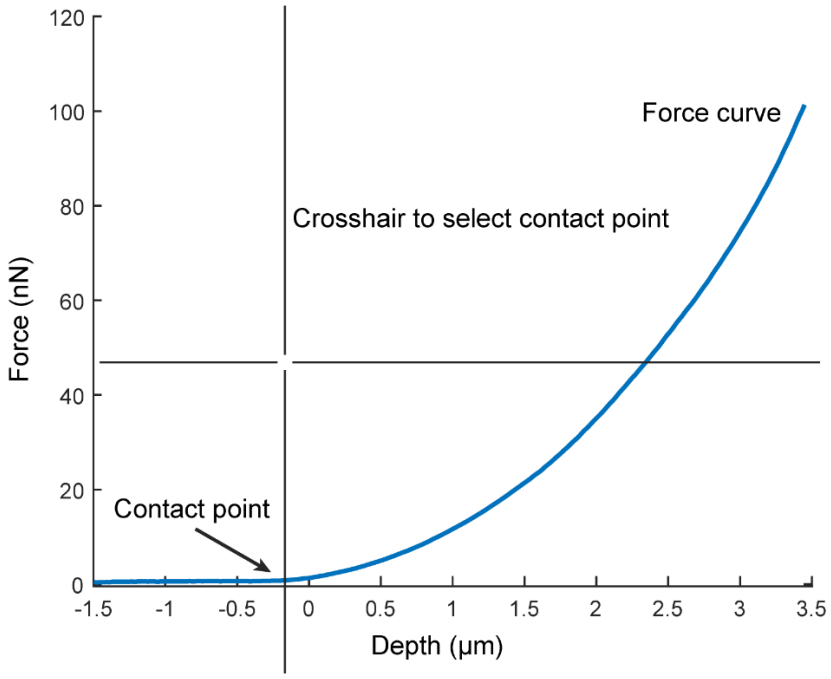

Figure 3.4. MATLAB ginput function allowed for manual selection of the contact point of the force curve. Any points along the x-axis less than the contact point were trimmed.

3.3 Applicability of the Hertz Model

The Hertz contact model is based on certain simplifying assumptions. It assumes that the yield stress of either contacting material is not exceeded, the load is normal to the contact plane, the contact area is very small compared to the dimensions of the contacting solids, surface roughness is negligible, and the contacting materials are at rest and in equilibrium [36]. To conform the experiments to the validity of the model, indents were conducted at a slow rate and were considered quasi-static [37]. The model was applied over specific depths to keep the contact area small compared to other dimensions [24]. The results of the indentation tests confirm the use of the Hertz model as a means of systematically comparing these curves. After close to 15,000 indents, there was nearly identical behavior across all force curves. Interactions between the probe and elements on the surface like large asperities would be made apparent by a force drop on the

curve, but the extension portion of the curves remains smooth throughout the motion of the probe, seen in Figure 3.5. Curves were similar to each other even across multiple locations on both unworn and worn surfaces. This consistent behavior confirms no interference due to surface features during the experiments.

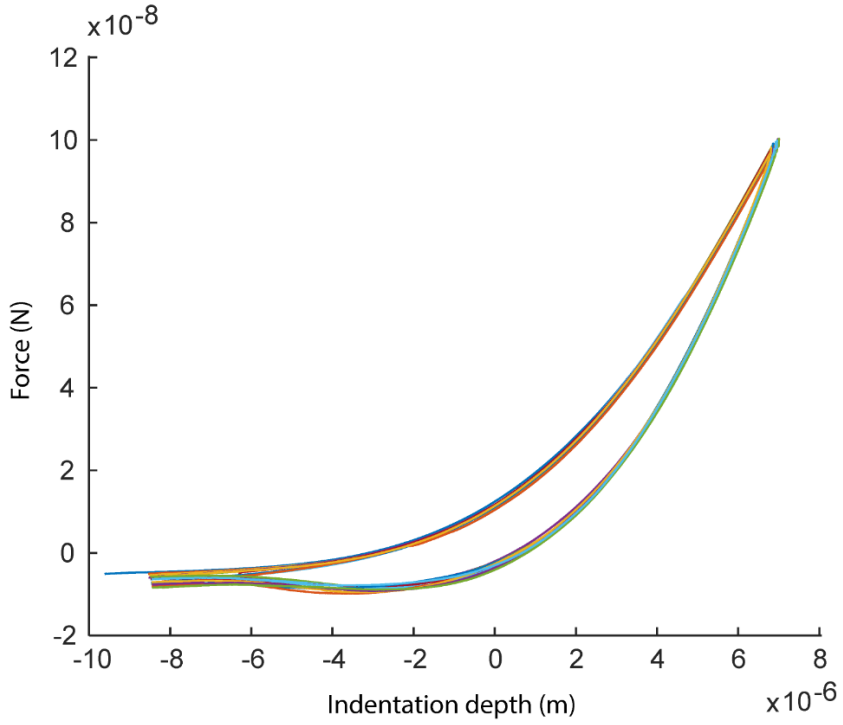

Figure 3.5. An overlay of ten force curves from a representative unworn sample prior to any shifting, trimming, or fitting.

CHAPTER 4: RESULTS AND DISCUSSION

This chapter presents the results of the wear experiments. Results from a single wear experiment for two characteristic samples are presented first. The findings from these experiments motivated the longitudinal experiments, which quantified the changes experienced by the hydrogel surface due to repeated applications of wear. A discussion of the physical mechanism explaining these observations is also presented.

4.1 Wear Experiments

In initial experiments, a single unworn sample was tested in the AFM, worn with 1000 grit sandpaper, and then tested again the AFM. The force curve data from the unworn and subsequently worn hydrogel was evaluated in MATLAB, and the values of elastic moduli across the surface were examined to determine the effects abrasive wear had on the hydrogel.

The values of the elastic moduli can be seen in Figure 4.1 (a) and (b). These graphs show a box and whisker plot distribution of elastic moduli values. The middle 50% of values are contained within the box while the whiskers stretch another 1.5 times the interquartile range. Any symbols outside the whiskers represent outliers while the line across the box denotes the median. The median value for the unworn hydrogel in Figure 4.1 (a) was 1.31 kPa, but after wear, the median was 2.26 kPa, an increase of 73%. Similarly, for the hydrogel sample in Figure 4.1 (b), the median value was 1.55 kPa on an unworn gel but increased to 2.55 kPa after the application of wear, an increase of 65%. Along with an increase in the median elastic modulus value after wear, the distribution of values also widened, seen in the size of the boxes and extension of the whiskers. On the sample in (a), the range of modulus values was 1.14 kPa on an unworn hydrogel which increased to 2.35 kPa following wear. In the sample in Figure 4.1 (b), this range increased from 1.91 kPa pre-wear to 2.35 kPa post-wear.

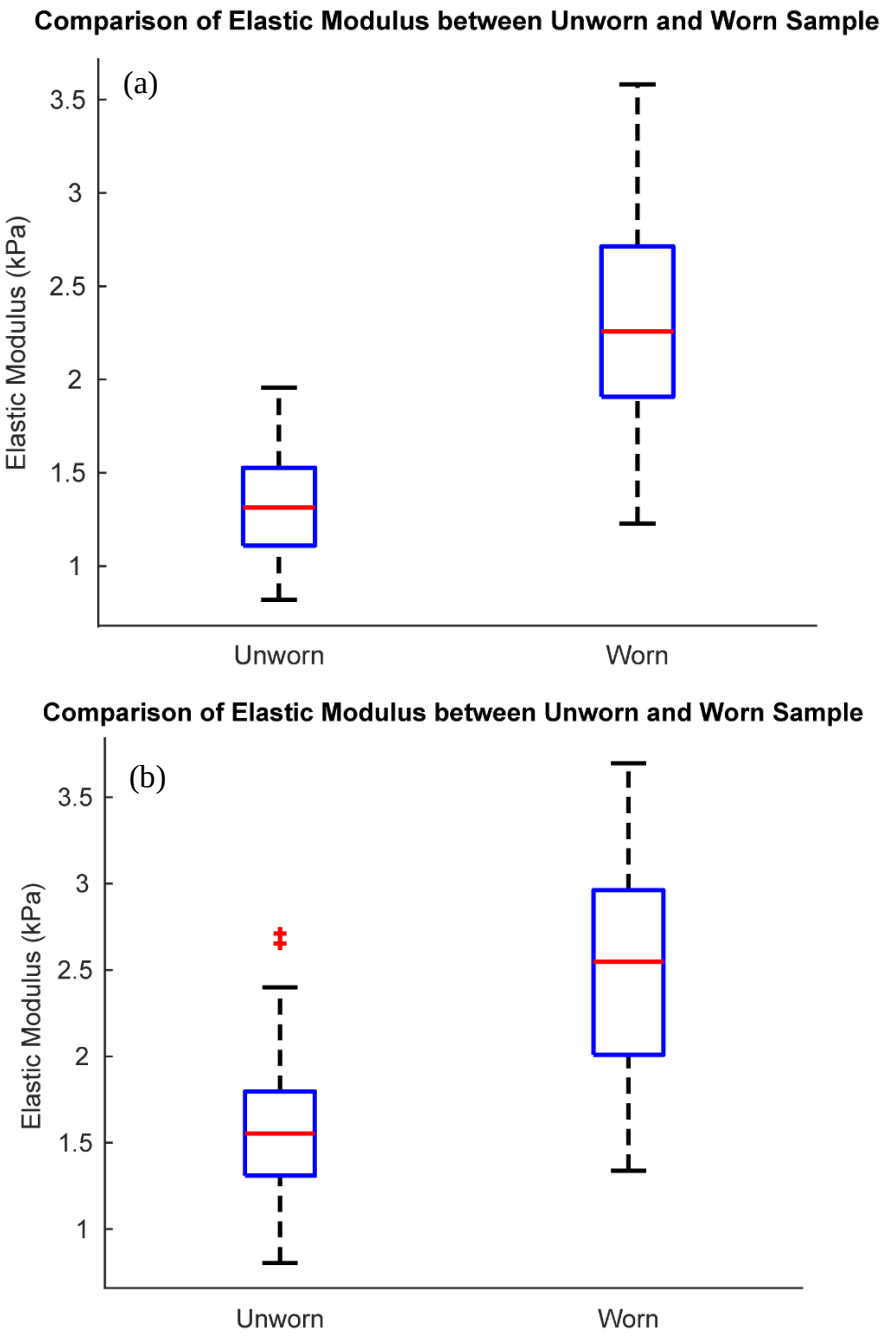

Figure 4.1. (a) and (b). Box and whisker plots showing the distribution of elastic modulus values on two individual representative samples before and after wear. The results from these preliminary experiments motivated the longitudinal experiments to see if this behavior of increased stiffness post-wear was observable after multiple applications of wear.

These observations suggested physical changes to the hydrogel following wear. First, the topography of the surface became less uniform. A smaller initial distribution in modulus values showed a uniformity across the unworn surface that changed after the application of wear. This distribution can also be seen in Figure 4.2, which shows the results of the force map array: elastic moduli from 100 force curves across the hydrogel surface. A similar increase in both the median value and the range of values of the elastic moduli can be seen in this figure.

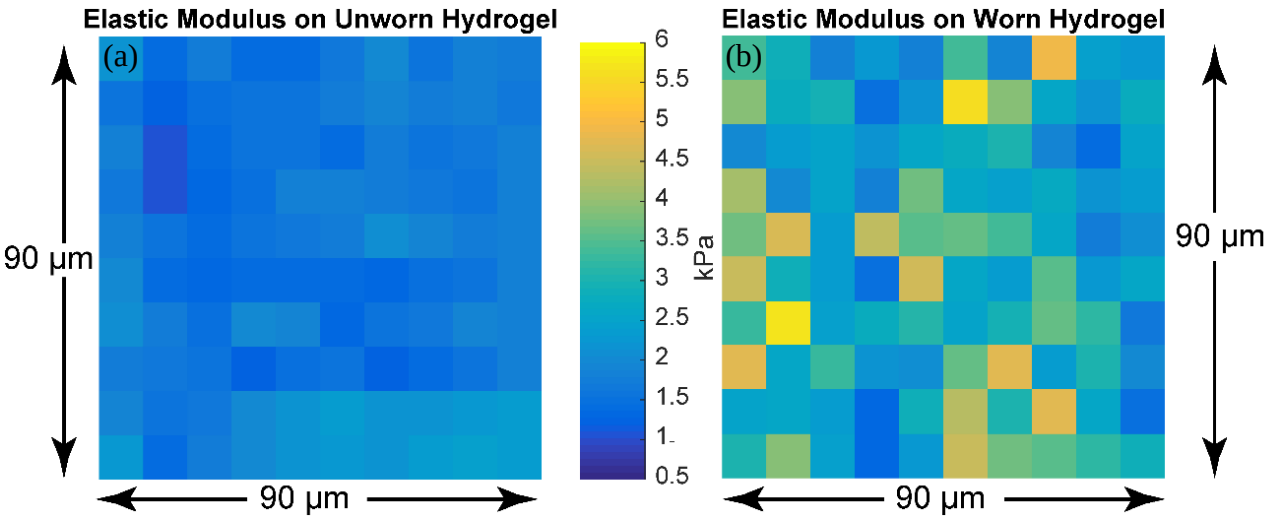

Figure 4.2. Scatter plot showing the elastic modulus values for each of 100 force curves in a 90 µm x 90 µm area indented through the force mapping procedure. The map in (a) shows the values on an unworn sample while the map in (b) shows the values on the same sample following wear.

A second change apparent from these tests was that the surface, on average, became stiffer after wear. An important conclusion drawn from this observation was that a soft surface layer had been stripped away by the abrasive wear. A pristine, unworn sample had a surface with relatively uniform topography and stiffness. Once this surface was removed, the worn sample was stiffer and rougher, and regions across the surface became dissimilar to each other.

4.2 Longitudinal Experiments

The longitudinal experiments quantified how the hydrogel changed over time. The driving hypothesis for these experiments was that abrasive wear completely removed a soft surface to reveal a stiffer layer underneath, but that a new soft surface layer would later appear. If the free surface was re-hydrated, it may also get less stiff. Figure 4.3 shows the results of this progression described in Chapter 2 (Figure 2.5). A comparison of the distribution of values on the unworn sample (left) and the worn sample (right) showed a similar trend of a stiffer, less homogeneous surface. The distribution of values was more regular at the start of each experiment on different days. Instead of retaining the same properties seen after wear, the surface properties seemed to return to a similar state as the unworn sample.

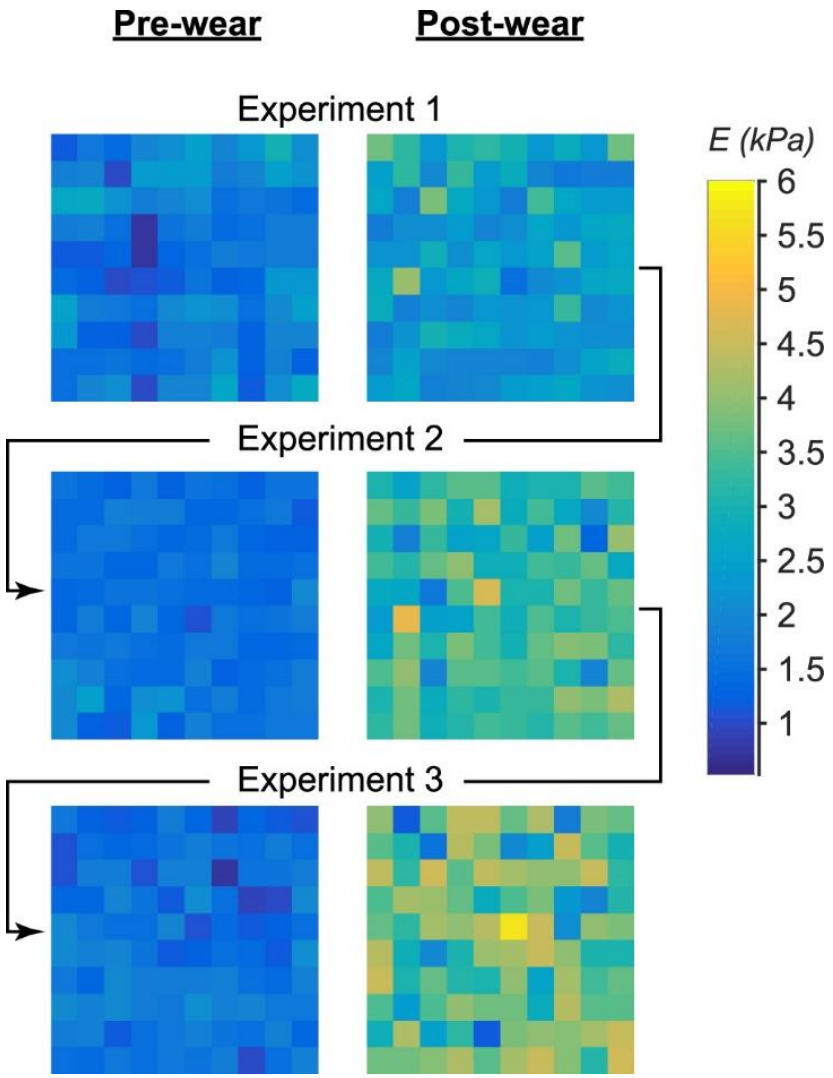

Figure 4.3. Contour maps showing the fitted elastic modulus distribution over the 90 μm x 90 μm area on each hydrogel surface from the quasistatic nanoindentation measurements. In each of the three serial experiments with ~72 hours recovery time in between, the average elastic modulus increased after the application of abrasive wear by 1000 grit sandpaper. The magnitude of increase appeared to increase with subsequent experiments, and the range of values also increased.

Figure 4.4 shows another set of box plots for the same sample in Figure 4.3. An oscillating progression of increase and decrease in elastic moduli values can be observed. Abrasive wear both increased the stiffness of the surface and widened the distribution of modulus values. However, after three days underwater, the sample became less stiff and the range of elastic modulus values

decreased. This observation suggested that hydrogels were self-regenerative. That is, given time to recover underwater, the surface layer seemed to re-swell, at least partially reversing the stiffening effects of wear. The mechanism to explain these results was that abrasive wear removed a soft, swollen surface layer. Time underwater, however, allowed the recently exposed stiffer bulk to swell and return to a surface layer similar to the original surface layer of a new sample.

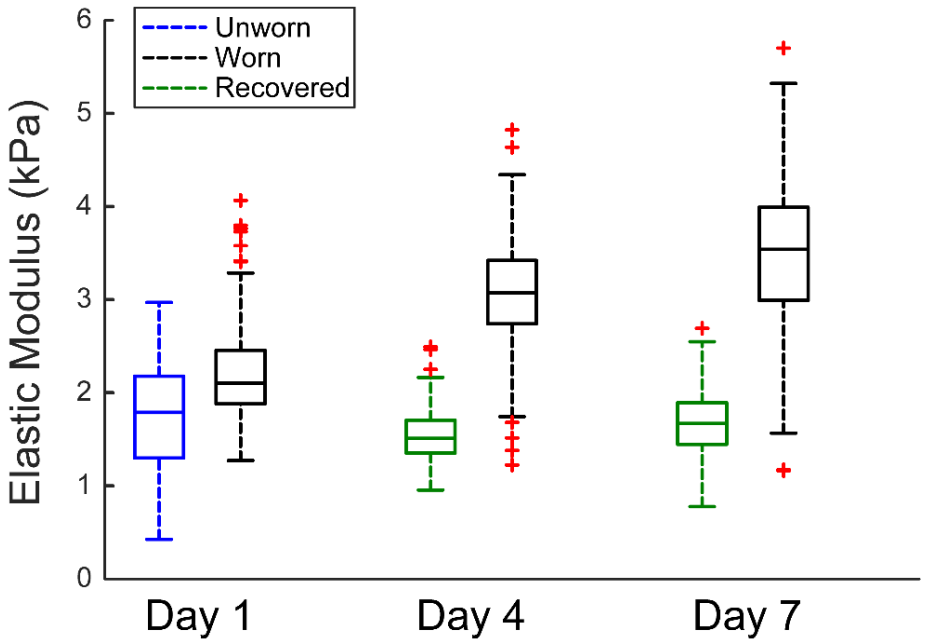

Figure 4.4. Box-and-whisker plots of the modulus of elasticity over longitudinal experiments at the nanoscale. All measurements were identical. Each box and whisker plot represents two maps of 100 indentations each. This quantifies the increased modulus after wear, and the increasing variability in modulus after three experiments, performed over seven days. After recovery in a water bath for three days, the median elastic modulus recovered to the lower value of E~1.6 kPa both times.

Figure 4.5 shows box plots for a longitudinal experiment conducted on a second characteristic sample. As in previous experiments, the surface elastic modulus increased after the application of wear, and the distribution of values widened. In this experiment, the post-wear

sample did not have as drastic an increase in the median value of the modulus as the sample shown in Figure 4.4, though there was an increase in the ranges of modulus values. On Day 4, for example, the range of modulus values is 0.96 kPa on the recovered gel, but after an application of wear, this range increased to 2.8 kPa. In the recovered gel (blue) on days four and seven, the distribution of values was much smaller than the distribution of the post-wear sample on those same days. This implied the regenerated surface was smoother and the topography more uniform than the surface roughened by abrasive wear.

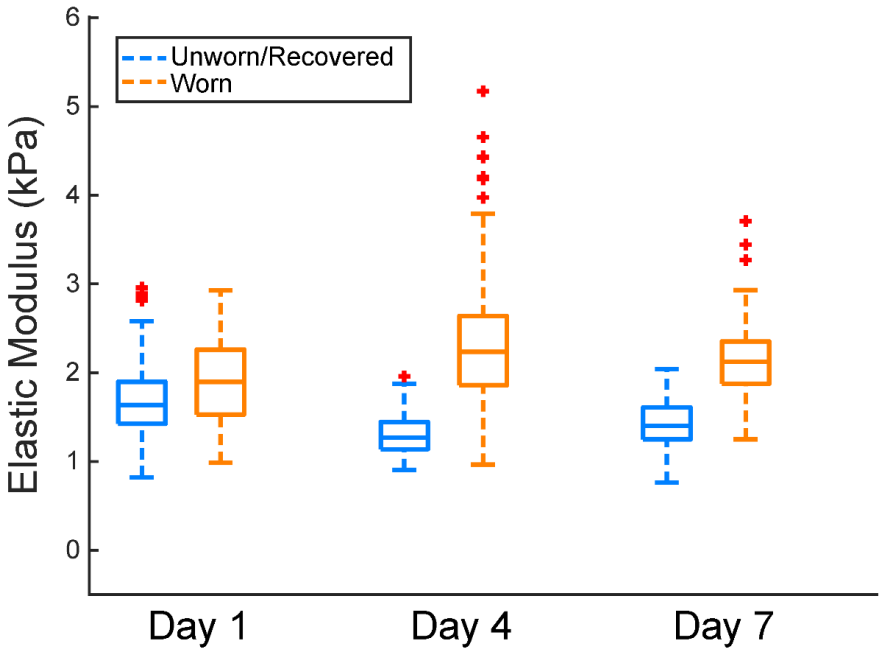

Figure 4.5. Box-and-whisker plots of the modulus of elasticity over longitudinal experiments at the nanoscale. The same procedure was followed for the sample shown in Figure 4.4. Results are consistent, though not as pronounced.

CHAPTER 5: CONCLUSIONS

Wear had measurable effects on hydrogel surface stiffness. It increased surface stiffness and widened the distribution of elastic modulus values. After re-equilibrating in water, the hydrogel surface properties resembled the values as found on a fresh, unworn hydrogel: surface elastic modulus decreased, and the surface topography became more homogeneous. These results demonstrated that hydrogel surfaces were self-regenerating. Wear removed a soft swollen surface layer and revealed a stiffer bulk; however, this layer was recoverable. Hydrogel surface stiffness was not permanently altered by abrasive wear, and samples could withstand repeated applications of wear while still retaining their mechanical properties. However, wear may have liberated particles from the surface whose morphology and properties were unknown. This research in applied surface wear uncovered unexpected surface mechanics and provided another step toward the implementation of hydrogels in load-bearing applications within the human body.

CHAPTER 6: SUPPLEMENTARY FINDINGS

6.1 Attempts at Surface Imaging

Throughout the course of this research, different techniques were used to get an image of the surface of the hydrogel both before and after wear. A visual confirmation of the observed physical changes would help explain the mechanism by which these changes occurred but proved consistently difficult to obtain. The first attempts were with a sharp probe in the Asylum MFP-3D AFM where the indentation experiments were performed. The sharp tip never adequately identified the surface and at higher forces likely sliced through the top layer of the sample. Applying less force or smaller oscillations in tapping mode caused the probe to get stuck in the surface.

A second attempt was made with a Park NX10 SICM Module (Park Systems, Korea). This featured a scanning ion conductance module attached to an AFM specifically designed for non-contact soft material imaging in aqueous environments. This module applied no force to the sample and instead detected the surface by measuring changes in electrical current. However, the probe was unable to detect a change before puncturing the surface, possibly because there was not a significant difference between a sample which was 92 wt.% water and its surroundings.

Another attempt was using Raman spectroscopy (Raman 11, Nanophoton, Japan) which measured scattering light as it interacted with a sample. Imaging a transparent sample in water returned no discernible scattering, so fluorescent dye was added on top of a worn sample. In this case, the microscope recognized some difference between the bulk of the hydrogel and the dyed water on top, but it was unable to image the surface with a high enough resolution to identify any sort of wear pattern. A final attempt at imaging the surface was with a 3D optical profiler (Keyence, Japan). Like other optical techniques, it also struggled with identifying the surface of a transparent sample in fluid.

6.2 Recommended future work

One of the primary conclusions from this thesis is that the hydrogel surface is regenerative, that is: an application of wear measurably changes the surface properties, but these properties are recoverable. After a period under water, the surface elastic modulus returns to a similar range of values as before any wear is applied. This implies that the surface changes, likely swelling in areas exposed by the sandpaper. There are some additional experiments that could provide supporting data for these conclusions. The next step is to see how these surface properties compare to those in the bulk and if newly created surfaces develop the same properties as the original surface.

Bulk property measurement: These experiments will focus on quantifying the stiffness and friction response of a region originally within the bulk of the hydrogel. These experiments are time-sensitive and will have to be completed quickly before the newly-created surface has time to swell. Using a recently-developed hydrogel-slicing mechanism, the user can make a series of cuts across the width of a sample and expose a new surface for characterization. Friction and indentation tests on this new surface can be performed, and the results can be compared to the values found on the original surface of a gel. The elastic modulus on a surface recently within the bulk of the sample will likely be stiffer than that on an older surface. The polymer chains within the bulk will be more tightly packed together, leading to a higher apparent elastic modulus. With a free surface and exposure to water, these chains will shift farther apart, the surface will swell, and the stiffness will decrease.

Bulk-to-surface transition measurements: These experiments will seek to quantify the transition of a region between bulk and surface. Again, using the hydrogel-slicing mechanism, a user can create a new surface, position it under the microtribometer, and perform a series of force curves. With a pattern of indents consistently spaced over a long period of time, the elastic

properties of the sample can be characterized as the surface swells. Initial values will likely be higher, and over time the elastic modulus should decrease as the hydrogel swells. Results of this experiment will aid in understanding the speed at which water is absorbed by the hydrogel, and the point at which the surface saturates. Hopefully a critical point will be identifiable, and a clear distinction can be drawn between bulk and surface.

REFERENCES

[1] T. R. Hoare and D. S. Kohane, “Hydrogels in drug delivery: Progress and challenges,” *Polymer (Guildf).*, vol. 49, no. 8, pp. 1993–2007, 2008.

[2] G. Hoch, A. Chauhan, and C. J. Radke, “Permeability and diffusivity for water transport through hydrogel membranes,” *J. Memb. Sci.*, vol. 214, no. 2, pp. 199–209, 2003.

[3] A. C. Rennie, P. L. Dickrell, and W. G. Sawyer, “Friction coefficient of soft contact lenses: Measurements and modeling,” *Tribol. Lett.*, vol. 18, no. 4, pp. 499–504, 2005.

[4] C. M. Kirschner and K. S. Anseth, “Hydrogels in healthcare: From static to dynamic material microenvironments,” *Acta Mater.*, vol. 61, pp. 931–944, 2013.

[5] B. Ratner and A. Hoffman, “Synthetic hydrogels for biomedical applications,” in *ACS Symposium Series; American Chemical Society*, 1976.

[6] M. Ahearne, Y. Yang, and K. Liu, “Mechanical Characterisation of Hydrogels for Tissue Engineering Applications,” *Tissue Eng.*, vol. 4, pp. 1–16, 2008.

[7] J. Katta, M. Marcolongo, A. Lowman, and K. Mansmann, “Friction and wear behavior of poly(vinyl alcohol)/ poly(vinyl pyrrolidone) hydrogels for articular cartilage replacement,” *Wiley Intersci.*, 2007.

[8] A. C. Dunn, J. Manuel, Y. Huo, S. S. Perry, T. E. Angelini, and W. G. Sawyer, “Lubricity of Surface Hydrogel Layers,” pp. 371–378, 2013.

[9] M. Tokita and T. Tanaka, “Friction coefficient of polymer networks of gels,” *J. Chem. Phys.*, vol. 95, no. 6, pp. 4613–4619, 1991.

[10] T. Shoaib, J. Heintz, J. Lopez-Berganza, S. A. Egner, and R. M. Espinosa-Marzal, “Stick-slip friction reveals hydrogel lubrication mechanisms,” *Langmuir*, 2017.

[11] J. P. Gong, G. Kagata, Y. Iwasaki, and Y. Osada, “Surface dynamic friction of polymer gels,” *Chinese.J.Polym.Sci.*, vol. 18, no. 3, pp. 271–275, 2000.

[12] M. E. Freeman, M. J. Furey, B. J. Love, and J. M. Hampton, “Friction , wear , and lubrication of hydrogels as synthetic articular cartilage,” *Wear*, vol. 241, pp. 129–135, 2000.

[13] J. F. Archard, “Contact and rubbing of flat surfaces,” *J. Appl. Phys.*, vol. 24, no. 8, pp. 981–988, 1953.

[14] Zeus Industrial Products, “Friction and Wear of Polymers,” 2005.

[15] J. K. Lancaster, “Abrasive Wear of Polymers,” *Mater. Sci.*, vol. 4, pp. 223–239, 1969.

[16] S. H. Kim, A. Opdahl, C. Marmo, and G. A. Somorjai, “AFM and SFG studies of pHEMA-based hydrogel contact lens surfaces in saline solution : adhesion , friction , and the presence of non-crosslinked polymer chains at the surface,” *Biomaterials*, vol. 23, pp. 1657–1666, 2002.

[17] J. M. Lenhardt, M. T. Ong, R. Choe, C. R. Evenhuis, T. J. Martinez, and S. L. Craig, "Trapping a diradical transition state by mechanochemical polymer extension," *Science (80-.).*, vol. 329, no. 5995, pp. 1057–1060, 2010.

[18] L. Han *et al.*, "Tough, self-healable and tissue-adhesive hydrogel with tunable multifunctionality," *NPG Asia Mater.*, vol. 9, no. 4, 2017.

[19] A. Phadke *et al.*, "Rapid self-healing hydrogels," *Proc. Natl. Acad. Sci.*, vol. 109, no. 12, pp. 4383–4388, 2012.

[20] J. Kopecek and J. Yang, "Hydrogels as smart biomaterials," *Polym. Int.*, vol. 56, pp. 1078–1098, 2007.

[21] T. Takigawa, Y. Morino, K. Urayama, and T. Masuda, "Poisson's Ratio of Polyacrylamide (PAAm) Gels," *Polym. Gels Networks*, vol. 4, no. 1, pp. 1–5, 1996.

[22] A. K. Denisin and B. L. Pruitt, "Tuning the Range of Polyacrylamide Gel Stiffness for Mechanobiology Applications," *ACS Appl. Mater. Interfaces*, vol. 8, pp. 21893–21902, 2016.

[23] A. L. Daniel-Da-Silva, J. Moreira, R. Neto, A. C. Estrada, A. M. Gil, and T. Trindade, "Impact of magnetic nanofillers in the swelling and release properties of κ-carrageenan hydrogel nanocomposites," *Carbohydr. Polym.*, vol. 87, no. 1, pp. 328–335, 2012.

[24] P. C. Nalam, N. N. Gosvami, M. A. Caporizzo, R. J. Composto, and R. W. Carpick, "Nano-rheology of hydrogels using direct drive force modulation atomic force microscopy," *Soft Matter*, vol. 11, pp. 8165–8178, 2015.

[25] Bangs Laboratories, "Product Data Sheet 702." Fishers, IN, 2016.

[26] A. Fery, F. Dubreuil, and H. Möhwald, "Mechanics of artificial microcapsules," *New J. Phys.*, vol. 6, pp. 1–13, 2004.

[27] N. Ahmadi, L. M. Keer, and T. Mura, "Non-Hertzian contact stress analysis for an elastic half space-normal and sliding contact," *Int. J. Solids Struct.*, vol. 19, no. 4, pp. 357–373, 1983.

[28] Asylum Research, *MFP 3D SPM User Guide*, Version 13. 2013.

[29] Y. Lai and Y. Hu, "Soft Matter indentation on gels for spherical , conical and cylindrical indenters," *Soft Matter*, vol. 13, pp. 852–861, 2017.

[30] E. M. Darling, R. E. Wilusz, M. P. Bolognesi, S. Zauscher, and F. Guilak, "Spatial Mapping of the Biomechanical Properties of the Pericellular Matrix of Articular Cartilage Measured In Situ via Atomic Force Microscopy," *Biophys. J.*, vol. 98, no. 12, pp. 2848–2856, 2010.

[31] D. C. Lin, D. I. Shreiber, E. K. Dimitriadis, and F. Horkay, "Spherical indentation of soft matter beyond the Hertzian regime : numerical and experimental validation of hyperelastic models," pp. 345–358, 2009.

[32] D. Lee, M. M. Rahman, Y. Zhou, and S. Ryu, “Three-Dimensional Confocal Microscopy Indentation Method for Hydrogel Elasticity Measurement,” *Langmuir*, vol. 31, no. 35, pp. 9684–9693, 2015.

[33] ASTM International, *ASTM E438-92 (2018) Standard Specification for Glasses in Laboratory Apparatus*, E438 − 92. West Conshohocken, PA, 2018.

[34] MathWorks, “Evaluating Goodness of Fit,” *MATLAB Documentation*, 2018. [Online]. Available: https://www.mathworks.com/help/curvefit/evaluating-goodness-of-fit.html. [Accessed: 12-Apr-2018].

[35] MathWorks, “fit,” *Curve Fitting Toolbox Documentation*, 2018. [Online]. Available: https://www.mathworks.com/help/curvefit/fit.html. [Accessed: 15-Apr-2018].

[36] G. Stachowiak and A. Batchelor, *Engineering Tribology*, Fourth Edi. Kidlington, Oxford, UK: Elsevier, 2014.

[37] J. Jefferson Andrew, V. Arumugam, C. Ramesh, S. Poorani, and C. Santulli, “Quasi- static indentation properties of damaged glass/epoxy composite laminates repaired by the application of intra-ply hybrid patches,” *Polym. Test.*, vol. 61, pp. 132–145, 2017.